

Behavior of 2^3S metastable state He atoms in low-temperature recombining plasmas

Shin Kajita

*Institute of Materials and Systems for Sustainability,
Nagoya University, Nagoya 464-8603, Japan**

Tadashi Tsujihara

Graduate School of Engineering, Nagoya University, Nagoya 464-8603, Japan

Mitsutoshi Aramaki

College of Industrial Technology, Nihon University, Chiba 275-8575, Japan

Hennie van der Meiden

*FOM Institute DIFFER, Dutch Institute for Fundamental Energy Research,
De Zaale 20, 5612 AJ, Eindhoven, Netherland*

Oshima Hiroshi, Noriyasu Ohno, Hirohiko Tanaka

Graduate School of Engineering, Nagoya University, 464-8603, Japan

Ryo Yasuhara, Tsuyoshi Akiyama

National Institute for Fusion Science, Gifu 509-5202, Japan

Keisuke Fujii and Taiichi Shikama

Graduate School of Engineering, Kyoto University, Kyoto 615-8540, Japan

(Dated: May 20, 2017)

Abstract

We measured the electron density and temperature using laser Thomson scattering and metastable state (2^3S) of He atoms using laser absorption spectroscopy in the detached recombining plasmas in the divertor simulator NAGDIS-II. Using the measured electron density and temperature combined with the particle trajectory trace simulation, we discussed the behavior of the metastable state He atoms based on comparisons with the experimental results. It is shown that the metastable states atoms are mainly produced at the peripheral region of the plasma column, where the temperature is lower than the central part, and diffused in the vacuum vessel. It was shown that the **0D model** is not valid and the transport of the metastable states is to be taken into account for the population distribution of He atoms valid in the detached plasmas.

PACS numbers:

*Electronic address: kajita.shin@nagoya-u.jp

I. INTRODUCTION

Plasma detachment is thought of as a method to control particle/heat loads on divertor materials [1–3]: particle recycling and ion-neutral friction in the near surface plasma leads to cooling and temperature gradients along the magnetic field lines. Diagnostics of the low temperature recombining plasmas is required for detailed understanding of the mechanisms involved. However, in the electrostatic probe method, an anomaly is identified in the current voltage characteristics [4–7], and the introduction of laser Thomson scattering (LTS) requires special care [8–10], since the temperature is much lower than 1 eV.

In addition, optical emission spectroscopy can be a convenient measurement method without making any disturbance on plasmas. Helium line intensity ratios [11–13] have been utilized to determine the plasma parameters. However, there are some potential factors to change the population distribution. One is the effect of radiation trapping [13–16], which increases directly the n^1P population, where n is the principal quantum number, and the populations of the surrounding states can be enhanced consequently [17]. To include the effect of radiation transport, optical escape factor [13–16, 18, 19] has been used, and, moreover, models were developed to include photon excitation directly [17, 20]. In addition to the radiation transport, the density of the metastable atoms are essential in terms of the validity of the quasi-steady-state (QSS) approximation [12, 21]. In recombining plasmas, transport of metastable states atoms would not be neglected, because the extinction rate by electron impact excitation decreases significantly with decreasing the electron temperature. Thus, it is of importance to investigate the behavior of metastable He atoms in detached plasmas. By detailed analysis of the 2^3S - 2^3P transition spectral line shape, the 2^3S density can be measured by considering the effect of self-absorption [22, 23]; it requires high wavelength resolution detector such as a tunable Fabry-Perot etalon.

In this work, we developed a laser absorption spectroscopy (LAS) to measure the 2^3S atoms and an advanced LTS system to measure the electron density and temperature in the divertor simulator NAGDIS-II (Nagoya Divertor Simulator). After description of measurement setups, measured plasma density and temperature and the 2^3S density of He atoms in the detached plasmas are presented. To understand the behavior of the metastable atoms, we simulate the transport of the particles with including the collisions using a Monte Carlo method. Based on the experimental and numerical simulation results, we discuss the behav-

ior of the metastable state atoms in the detached plasmas in the NAGDIS-II. It is shown that transport of 2^3S is inevitable to understand the behavior in detached recombining plasmas.

II. SETUP

A. Plasma device

In the linear divertor simulator NAGDIS-II device, high density plasmas are produced in a direct current discharge with a heated LaB_6 cathode as presented in [1]. Magnetic field of up to ~ 0.25 T makes a linear plasma with the length of ~ 2.5 m. In the attached plasmas, the plasma diameter was typically 2 – 3 cm, but it increased in detached plasmas similar to the cases in PISCES-A [6]. In the present study, the magnetic field strength was 0.1 T. During the diffusion along the magnetic field line, the plasma temperature gradually decreases and recombination processes dominate the ionization when the temperature is sufficiently decreased. Typically, the strong recombination was initiated when the temperature is lower than < 1 eV [24].

B. Laser Thomson scattering system

An LTS system was developed for the NAGDIS-II. An Nd:YAG laser (Continuum: SLII-10) at the wavelength of 532 nm with the pulse width of 5-6 ns and the pulse energy of ~ 0.3 J at 532 nm was used combined with a spectrometer. The repetition rate of the laser pulse is 10 Hz. Figure 1(a) shows a schematic of the laser path and the collection optics. Before introducing the laser to the vacuum chamber, polarization was controlled by a half-waveplate and a cubic polarizer, so that the scattering signal can be effectively collected from the upper port. The diameter of the laser beam was expanded with a beam expander from 6 to ~ 12 mm, and, then, the laser beam was focused around the center of the vacuum chamber with a focusing lens. Two baffle plates were introduced in the injection port after a Brewster window: one (critical aperture) was just after the Brewster window, and the other one (subcritical aperture) was arranged at closer to the plasma, similar to the arrangement of the LTS in MAGNUM-PSI [10]. Laser beam was terminated with a laser beam dump. An optical bundle fiber (core diameter of $230 \mu\text{m}$ with 25 channels) and a doublet lens with the focal length of 750 mm was used to collect the scattered photons. The spatial resolution

of the measurement was ~ 1 mm. To reduce the stray light, viewing dump was arranged at the end of the field of view.

Figure 1(b) shows a schematic of the spectrometer. The photons collected are transferred through the optical fiber to the spectrometer. The spectrometer is composed of a volume phase holographic grating (2600 l/mm) and two camera lenses. The high etendue spectrometer was developed based on prototypes for MAGNUM-PSI [10] and the Large Helical Device (LHD) [25]. The introduced light is collimated with a camera lens (SIGMA, APO 300 mm F2.8 EX, focal length: 300 mm; F-number: 2.8). The collimated light transmits a custom made transmission grating (Wasatch Photonics, size: 135×100 mm²), and the diffracted light beam is focused with another camera lens (Canon, EF 200 mm F2L, focal length: 200 mm; F-number: 2.0). An image intensified charge coupled device (ICCD) (Andor: iStar) with GENIII type image intensifier was used for the detector. A slit is equipped at the face of optical fiber to increase the resolution in wavelength; however, we opened the slit wider than the fiber diameter to increase the number of photons rather than increase the wavelength resolution at the moment.

C. Laser absorption spectroscopy

Figure 2 shows a schematic of the LAS system. A distributed feedback (DFB) laser at ~ 1083 nm for $2^3\text{S}-3^3\text{P}$ is used for the laser. **The collimated laser had a diameter of 2-3 mm.** Doppler absorption spectra were obtained using the difference between the laser powers measured with and without the pass through the plasma. The main purpose to develop this measurement system is to measure the atomic temperature from the narrow Doppler broadening, and the details of the system and the temperature measurement results will be shown in elsewhere [26]. In this study, we focus on the 2^3S density measured from the absorption spectra.

III. MEASUREMENT RESULTS

A. Electron density and temperature measurements

Figure 3(a) shows the stray light signal, and Figs. 3(b) and (c) show typical TS spectrum in an attached ionizing plasma and a detached recombining plasma, respectively. It is seen

that the stray light spectrum was much narrower and stronger than the Thomson scattering signal. In both cases of Figs. 3(b) and (c), the discharge current was 60 A, but the gas pressure was 4.4 and 13.5 mTorr and the measurement position was at $r = 0$ and 11.7 mm, respectively. We can identify that strong stray light component exists, and the wavelength range (531.6-532.6 nm) was eliminated when performing fitting. The peak of the stray light was $\sim 2 \times 10^5$, which was out of the scales in Figs. 3(b) and (c), but the saturation of the detectors did not occur. Note that CCD pixels are binned for a fiber in the software. To obtain the spectrum, TS signals were averaged 300 times (30 s). The deduced density and temperature were, respectively, $5.6(\pm 0.2) \times 10^{18} \text{ m}^{-3}$ and $3.2 \pm 0.2 \text{ eV}$ in the attached plasma and $3.5(\pm 0.2) \times 10^{18} \text{ m}^{-3}$ and $0.29 \pm 0.03 \text{ eV}$ in the detached plasma.

Figures 4(a) and (b) show the radial profiles of the electron density and temperature, respectively, measured by the LTS. The discharge current was 60 A, and the gas pressure was 12.4 mTorr. The density had a hollow profile with a peak at 13 mm, and the central density was approximately half that at the peak. The temperature was $\sim 0.4 \text{ eV}$ at the center and 0.1-0.2 eV at the peripheral region. Here, the errors were deduced from the standard deviation of the values by conducting measurement more than once.

Figures 5(a) and (b) show the discharge current dependences of the electron density and temperature, respectively, at $r = 0$ and 10-15 mm (averaged values). The density increased approximately three times at $r = 0 \text{ mm}$ and 1.5 times at the peripheral region with increasing the current from 20 to 60 A. In the detached plasma, the neutral temperature was measured to be $\sim 0.1 \text{ eV}$ [26]. It was thought that thermal equilibrium between the plasma and neutral gas was achieved when significant recombination occurred.

B. 2^3S state density measurement

The absorption coefficient at the frequency ν , $\kappa(\nu)$, can be written as

$$\kappa(\nu) = -\frac{1}{l} \ln \left(\frac{I_{\text{out}}}{I_{\text{in}}} \right), \quad (1)$$

where l is the absorption length, and I_{out} and I_{in} are the input laser power and output laser power, respectively. Figure 6(a) shows typical absorption spectrum for $2^3\text{S}-3^3\text{P}$ transition in the detached plasma in NAGDIS-II. Here, $I_{\text{out}}/I_{\text{in}}$ was plotted as a function of detuning frequency. The spectrum was composed of two components at 276.732 and 276.734 THz, and

the ratio was 5 to 3 from the statistical weight. There is another line at 276.764 THz, but since the total absorption should be eight times lower than that in Fig. 6(a), we chose the spectrum around 276.73 THz. **By using the Eq. (1) and integrating the absorption coefficient over the wavelength, the lower state density, n_m , can be obtained from the following relation when the upper state density is much less than the lower state density:**

$$\int \kappa(\nu) d\nu = \frac{\lambda^2 g' A n_m}{8\pi g}, \quad (2)$$

where λ is the wavelength, g and g' are the statistical weight for the lower and upper states, respectively, and A is the spontaneous emission coefficient.

Figure 6(b) shows the discharge current dependence of the line integrated 2^3S density ($n_m l$) when the laser was aligned at the center of the plasma column. When we used the diameter of the vacuum vessel for l ($l = 0.17$), the density was estimated to be in the range of $4 - 7 \times 10^{16} \text{ m}^{-3}$. The integrated density increased with the discharge current when the discharge current was lower than 35 A and decreased when the discharge current was higher than 40 A. In the next section, the behavior of 2^3S atoms in the recombining plasmas is discussed based on the comparisons between the experiments and simulations including transport of metastable atoms.

IV. BEHAVIOR OF 2^3S STATE ATOMS

A. Influence of transport

Figure 7 shows the characteristic time of neutral transport in NAGDIS-II and the extinction time of the 2^3S state atoms calculated by the collisional radiative (CR) code developed by Dr. Goto [12] with changing the electron temperature from 0.1 to 2 eV at the electron density of 10^{19} m^{-3} . **Here, the extinction time is defined as the inverse of the extinction rate by electron impact excitation and de-excitation processes to the other states.** The extinction time increases with decreasing the electron temperature and longer than the typical radial residual time when the electron temperature was 0.2 eV when the electron density is $\sim 10^{19} \text{ m}^{-3}$. As was shown in Figs. 4 and 5, since the electron temperature becomes 0.1-0.2 eV in the detached plasmas in NAGDIS-II, it is likely that the transport of 2^3S states becomes important and **QSS approximation without transport (0D model)** would not be valid. On the other hand, in the attached plasmas, where the temperature is higher than several eV,

the transport of 2^3S states can be negligible, and **0D model** is likely to be valid, as was discussed in [13, 16].

B. Modeling

To demonstrate the influence of transport quantitatively, motion of the metastable atoms are calculated by using a simulation code developed based on a particle transport code [27]. The initial position of 2^3S states atoms is allocated from the production rate calculated by the CR model including recombining and ionizing components, and the velocity was determined based on the measured temperature (600-1200 K) [26]. To calculate the production rate, we used QSS approximation for simplicity. Also, the measured electron density was used for the ion density, and the neutral density was deduced from the gas pressure measured by a Baratron gauge. This QSS approximation may not be valid as we discussed later in a strict sense, and iterative calculation is required between the transport of particles and re-calculation of population distribution, because the variation in 2^3S state density alters the surrounding state population distribution, which again affects the production rate. However, for the first step, here we introduce the transport effect and discuss the influence in the first order.

The trace of He atoms were calculated in two-dimensional space by considering three-dimensional velocity space. Elastic collisions with neutrals are taken into account using a Monte Carlo method. The extinction was calculated at each step with the extinction rates calculated by the CR model. **In addition, because the recombining region is not axially uniform, we took into account the parallel transport with a Monte Carlo method assuming that the recombining region is 0.5 m. That is to say, an extinction process with the probability of $l/(\Delta t v_{\parallel})$ was introduced for each step, where l is the assumed length of the recombining region of 0.5 m, Δt is the time step in the simulation, and v_{\parallel} the parallel neutral velocity.** About 50000 particles were traced until almost all the particles disappeared, and the density profiles were obtained by accumulating the positions of particles until they disappeared. **There exists a plasma flow from the upstream to downstream at least for ions in NAGDIS-II as was measured previously [28]. The range of the Mach number was 0.1-0.6 in the central region; when increasing the gas pressure, the flow decreased and the flow reversal occurred in the peripheral region. Concerning neutrals, though it has yet to**

be identified, flow may exist as well. However, it is at the moment difficult to take that influence into account. It is necessary to develop 3D simulation model and conduct flow measurement as well as axial plasma profiles for that purpose.

When the metastable state atoms hit a wall, de-excitation occurs frequently. Recently, a measurement was conducted for Ar metastable atoms. It was shown that de-excitation rate was 85% by the collision to stainless steel [29]. Since we could not find reliable wall effects for He metastable atoms, we assumed that the de-excitation rate was the same as the Ar case. It is noted that the metastable state density only increased by several % comparing between 85 and 100% de-excitation rate cases; we can say that the ambiguity in the de-excitation rate does not have significant influence on the calculation.

Figure 8 shows calculated radial profiles of 2^3S profile at the discharge current of 20, 40, and 60 A. It is seen that the distribution has a hollow profile. This is probably because the extinction process of 2^3S by electron bombardment is still working at $r < 20$ mm, and the production rate higher at the peripheral region. Comparing the extinction rate and production rate at center (0 mm) and edge (22 mm), the extinction rate is approximately one order of magnitude greater at the center, and the production rate is approximately one order of magnitude greater at the edge. At the moment, the measurement was conducted at only at $r < 22$ mm, and the density was assumed to be decreased to be zero at the vacuum chamber. Although the calculated profile could be slightly altered when we conducted LTS at wider region, it would not change the hollow profile shape shown in Fig. 9. At the peripheral region, since no extinction occurs, the metastable atoms can exist.

C. Comparison

Figure 9 shows comparisons of experimentally obtained and calculated 2^3S densities as a function of the discharge current. For simulation with transport, the average density was plotted with an error bar, which represents the minimum and maximum densities in the profile, while CR model calculations represent local calculated densities without transport at center ($r = 0$ mm) and edge ($r = 10 - 15$ mm). Without transport, the calculated edge density is significantly greater than the experimentally obtained value, while the density at the plasma center is orders of magnitude less than the experimental value. When we took into account the transport effect, the averaged density was consistent with the experimental

value within a factor of two, indicating that the transport effect is significant to determine the behavior of the metastable states in detached recombining plasmas. For more detailed analysis, we have to take into account the axial variation of the electron density and temperature, and neutral density. In the present study, the position for LTS and LAS was 30 cm different. Moreover, because ionizing plasma and recombining plasma exist within 1 m in axial direction, the transport in the axial direction may be important.

The calculated radial profiles of 2^3S in Figure 8 indicated that de-excitation on wall is necessary to explain the 2^3S density. However, it is unlikely that the 2^3S metastable states atom influence on the global power balance. In NAGDIS-II, the ion saturation current is roughly 0.5 A/cm^2 before strong recombination, and the size of the plasma is 20 mm in radius. Thus, considering the ionization energy of 24.6 eV, the parallel heat flux is estimated to be $\sim 150 \text{ W}$. The heat flux can be dissipated by recombination processes or transferred to the downstream in parallel direction. After the recombination, the energy would be released by radiation or kinetic energy. Concerning the metastable atoms, assuming that the density was $5 \times 10^{16} \text{ m}^{-3}$ and the recombination region was 0.5 m, and using the thermal velocity at 1000 K the potential energy of 19.8 eV, the energy reached on the wall will be 0.5 W, which is less than 1% of the parallel heat flux of the plasma. However, this estimation also suggested that the heat flux to the wall would be significant if the ground state atoms had similar temperature as that of metastables; it is of importance to measure the temperature of the ground state atoms in future.

From the present study, it became obvious that **0D model** would not valid in detached plasmas; the effect of transport is to be taken into account for the behavior of 2^3S metastable atoms. It is likely that the population around the metastable states such as triplet states in $n = 2$ and 3 can be affected by the transport effects of the metastable states. In this experiments, a linear divertor simulator was used; the same will also be true for detached plasmas in fusion devices in general. In future, it would be of interest to investigate how the transport of metastable changes the validity of the spectroscopic diagnostics in detached plasmas. It is unlikely that the metastable atoms changes the Saha-Boltzman analysis, because it only uses emission from high energy states, typically $n > 7$ in NAGDIS-II [30], on which the metastable atoms are not influential. However, for the line intensity ratio analysis, there is a possibility that the transport of metastable atoms changes the applicability of the methods. For ex., emissions at 667.8, 706.5, and 728.1 nm are frequently used as the electron

density and temperature analysis [12]. Since 3^3S is close to 2^3S states, the emission at 706.5 nm can be more vulnerable to the variation in 2^3S density compared to the other line emissions. Further detailed investigation of the effects can be future work.

V. CONCLUSIONS

We have developed a laser Thomson scattering and laser absorption spectroscopy systems for detached plasmas (low temperature recombining plasmas) in the linear plasma divertor simulator NAGDIS-II. The electron temperature and density in the detached plasma were measured by laser Thomson scattering; the temperature was well below 1 eV and the density was on the order of 10^{18} m^{-3} at the position close to the target (~ 2 m from the plasma source). A DFB laser at ~ 1083 nm for 2^3S - 3^3P transition is used for the laser absorption spectroscopy to measure the density of the metastable state. The density was $4\text{-}7 \times 10^{16} \text{ m}^{-3}$ in average. To understand the behavior of the metastable state atoms, we developed a transport model which include collision effects using Monte Carlo method. It was found that from the comparison with the experiments and simulation, metastable states atoms were produced in the peripheral region of the plasma and transported toward the wall radially. It was shown that **quasi steady state (QSS) approximation without transport (0D model)** cannot be used in detached plasmas, because the extinction rate of the metastable states are so low due to the low temperature. The disturbance of the metastable state population may have influence on the population distribution around the states. Concerning a line intensity method using He I line emission intensity, it is necessary to check the validity of the method in the detached plasmas. It would be necessary to find appropriate line intensity which would not be influenced by the 2^3S population density. Or, it would be required for the 2^3S population density to be another free parameter in addition to the electron density and temperature, as was demonstrated in [20].

Acknowledgment

We thank Dr. Goto from NIFS for providing us the collisional radiative model of He atoms. This work was supported in part by a Grant-in-Aid for Scientific Research (B) 15H04229 and (A) 16H02440 from the Japan Society for the Promotion of Science (JSPS)

and NIFS@collaborative research program (NIFS15KOA032).

- [1] N. Ohno, D. Nishijima, S. Takamura, Y. Uesugi, M. Motoyama, N. Hattori, H. Arakawa, N. Ezumia, S. Krasheninnikov, A. Pigarov and U. Wenzel: Nucl. Fusion **41** (2001) 1055.
- [2] G. Federici, C. Skinner, J. Brooks, J. Coad, C. Grisolia, A. Haasz, A. Hassanein, V. Philipps, C. Pitcher, J. Roth, W. Wampler and D. Whyte: Nucl. Fusion **41** (2001) 1967.
- [3] A. Loarte, B. Lipschultz, A.S. Kukushkin, G.F. Matthews, P.C. Stangeby, N. Asakura, G.F. Counsell, G. Federici, A. Kallenbach, K. Krieger, A. Mahdavi, V. Philipps, D. Reiter, J. Roth, J. Strachan, D. Whyte, R. Doerner, T. Eich, W. Fundamenski, A. Herrmann, M. Fenstermacher, P. Ghendrih, M. Groth, A. Kirschner, S. Konoshima, B. LaBombard, P. Lang, A.W. Leonard, P. Monier-Garbet, R. Neu, H. Pacher, B. Pegourie, R.A. Pitts, S. Takamura, J. Terry, E. Tsitrone and the ITPA Scrape-off Layer, Divertor Physics Topical Group: Nuclear Fusion **47** (2007) S203.
- [4] R. D. Monk, A. Loarte, A. Chankin, S. Clement, S. J. Davies, J. K. Ehrenberg, H. Y. Guo, J. Lingertat, G. F. Matthews, M. F. Stamp and P. C. Stangeby: J. Nucl. Mater. **241-243** (1997) 396.
- [5] N. Ezumi, N. Ohno, K. Aoki, D. Nishijima and S. Takamura: Contrib. Plasma Phys. **38** (1998) S31.
- [6] E. M. Hollmann, C. Brandt, B. Hudson, D. Kumar, D. Nishijima and A. Y. Pigarov: Physics of Plasmas **20** (2013) 093303.
- [7] Y. Hayashi, K. Jesko, H. van der Meiden, J. Vernimmen, T. Morgan, N. Ohno, S. Kajita, M. Yoshikawa and S. Masuzaki: Nuclear Fusion **56** (2016) 126006.
- [8] A. Okamoto, S. Kado, S. Kajita and S. Tanaka: Rev. Sci. Instrum. **76** (2005) 116106.
- [9] F. Scotti and S. Kado: J. Nucl. Mater. **390-391** (2009) 303.
- [10] H. J. van der Meiden, A. R. Lof, M. A. van den Berg, S. Brons, A. J. H. Donné, H. J. N. van Eck, P. M. J. Koelman, W. R. Koppers, O. G. Kruijt, N. N. Naumenko, T. Oyevaar, P. R. Prins, J. Rapp, J. Scholten, D. C. Schram, P. H. M. Smeets, G. van der Star, S. N. Tugarinov and P. A. Zeijlmans van Emmichoven: Review of Scientific Instruments **83** (2012) 123505.
- [11] B. Schweer, G. Mank, A. Pospieszczyk, B. Brosda and B. Pohlmeier: J. Nucl. Mater. **196-198** (1992) 174.

- [12] M. Goto: *J. Quantitative Spectroscopy and Radiative Transfer* **76** (2003) 331.
- [13] S. Kajita, N. Ohno, S. Takamura and T. Nakano: *Phys. Plasmas* **13** (2006) 013301.
- [14] S. Sasaki, S. Takamura, S. Watanabe, S. Masuzaki, T. Kato and K. Kadota: *Rev. Sci. Instrum.* **67** (1996) 3521.
- [15] Y. Iida, S. Kado, A. Okamoto, S. Kajita, T. Shikama, D. Yamasaki and S. Tanaka: *J. Fus. Res. SERIES* **7** (2006) 123.
- [16] D. Nishijima and E. M. Hollmann: *Plasma Phys. Control. Fusion* **49** (2007) 791.
- [17] S. Kajita and N. Ohno: *Rev. Sci. Instrum.* **82** (2011) 023501.
- [18] Y. Iida, S. Kado, A. Muraki and S. Tanaka: *Rev. Sci. Instrum.* **81** (2010) 10E511.
- [19] Y. Iida, S. Kado and S. Tanaka: *Physics of Plasmas* **17** (2010) 123301.
- [20] K. Sawada, Y. Yamada, T. Miyachika, N. Ezumi, A. Iwamae and M. Goto: *Plasma Fusion Research* **5** (2010) 001.
- [21] T. Fujimoto: *J. Quantitative Spectroscopy and Radiative Transfer* **21** (1979) 439.
- [22] T. Shikama, S. Ogane, H. Ishii, Y. Iida and M. Hasuo: *Japanese Journal of Applied Physics* **53** (2014) 086101.
- [23] T. Shikama, S. Ogane, Y. Iida and M. Hasuo: *Journal of Physics D: Applied Physics* **49** (2016) 025206.
- [24] A. Y. Pigarov and S. Krasheninnkov: *Phys. Lett. A* **222** (1996) 251.
- [25] K. Fujii, S. Atsumi, S. Watanabe, T. Shikama, M. Goto, S. Morita and M. Hasuo: *Review of Scientific Instruments* **85** (2014) 023502.
- [26] M. Aramaki, T. Tsujihara, S. Kajita, N. Ohno, (in preparation).
- [27] S. Kajita, S. Kado, N. Ohno, S. Takamura, K. Kurihara and Y. Kuwahara: *Phys. Plasmas* **14** (2007) 103503.
- [28] E.-K. Park, H.-J. Woo, K.-S. Chung, H. Tanaka, S. Kajita and N. Ohno: *Current Applied Physics* **12** (2012) 1497 .
- [29] Z.-B. Wang, J.-T. Li, X.-M. Zhu and Y.-K. Pu: *Journal of Physics D: Applied Physics* **48** (2015) 105203.
- [30] E. M. Hollmann, D. G. Whyte, D. Nishijima, N. Ohno, Y. Uesugi and N. Ezumi: *Physics of Plasmas* **8** (2001) 3314.

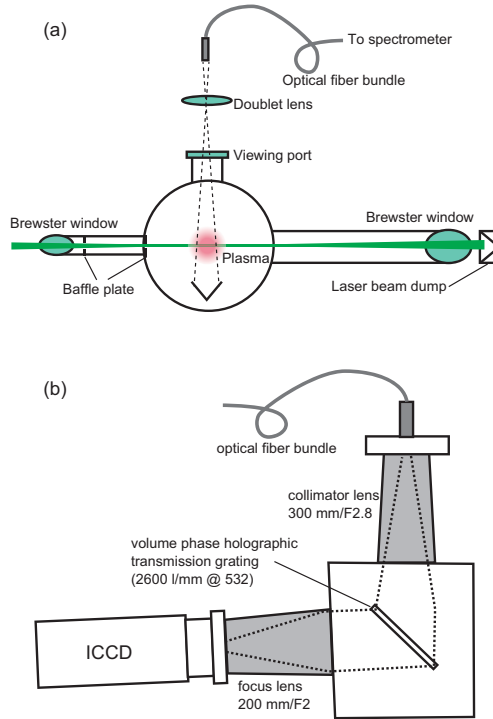


FIG. 1: (a) A schematic of the laser path and the collection optics for the LTS in the NAGDIS-II device, and (b) a schematic of the spectrometer for the LTS.

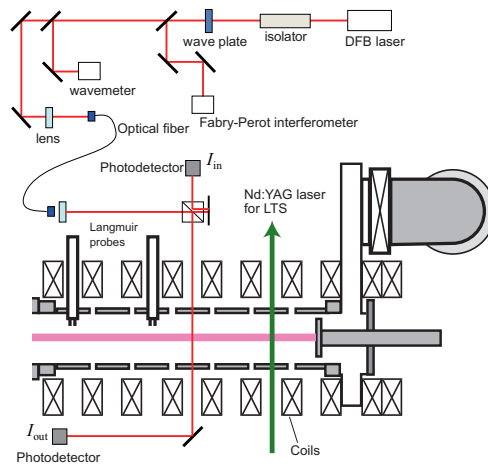


FIG. 2: A schematic of the LAS system in NAGDIS-II.

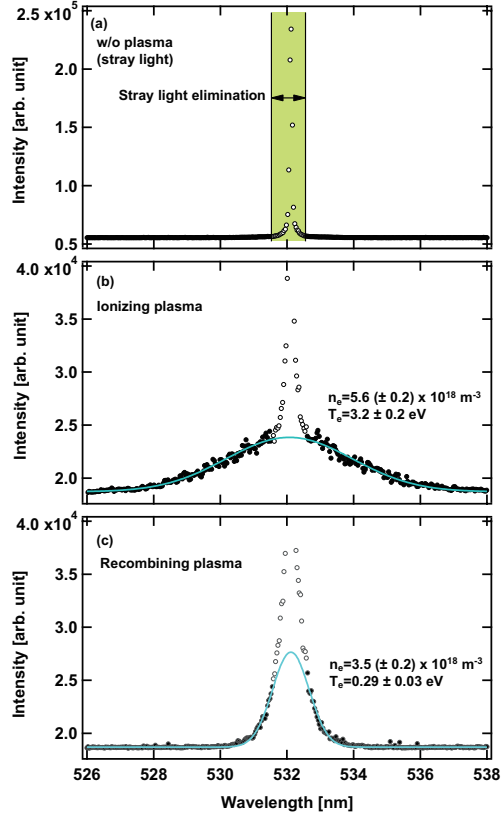


FIG. 3: Typical (a) stray light and TS spectrum in (b) an attached ionizing plasma and (c) a detached recombining plasma, respectively.

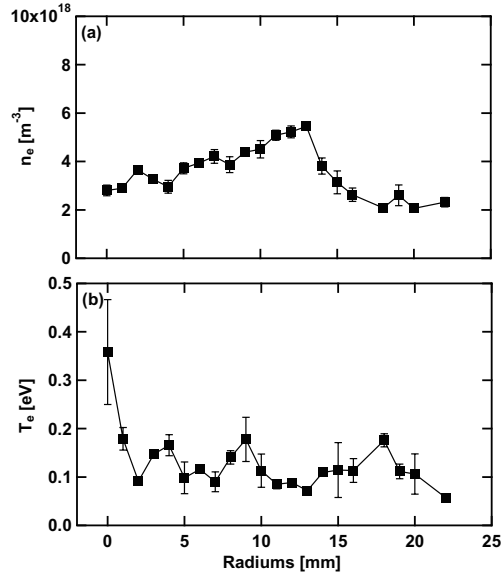


FIG. 4: Radial profiles of (a) the electron density and (b) temperature measured by the LTS.

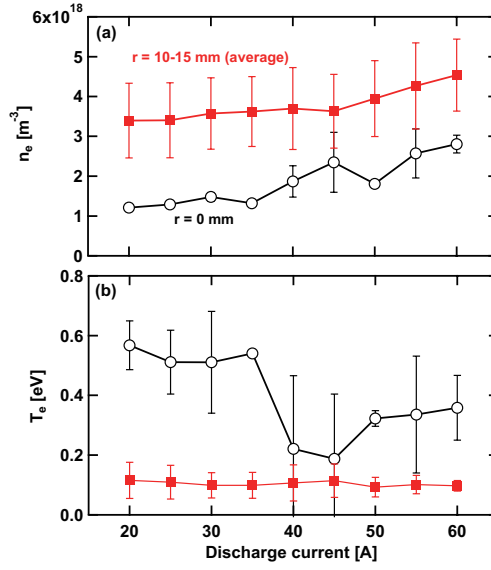


FIG. 5: Discharge current dependences of (a) the electron density and (b) temperature at $r = 0$ and 10-15 mm (averaged values).

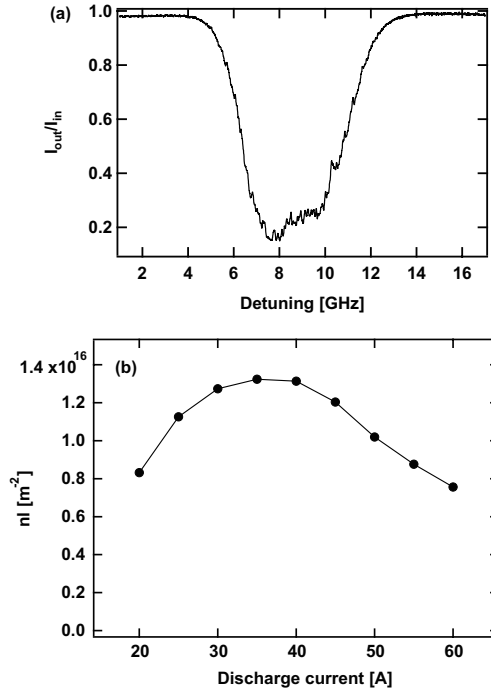


FIG. 6: (a) a typical absorption spectrum for $2^3\text{S}-3^3\text{P}$ transition in the detached plasma in NAGDIS-II and (b) the discharge current dependence of the line integrated 2^3S density when the laser was aligned at the center.

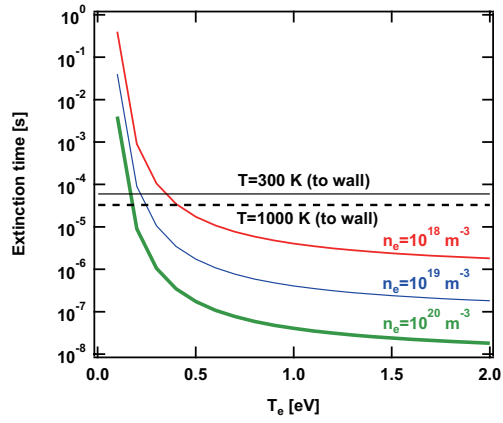


FIG. 7: The characteristic time of neutral transport in NAGDIS-II and the extinction time of the 2^3S state atoms as a function of the electron temperature.

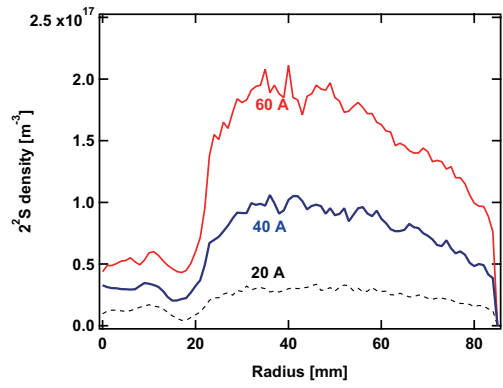


FIG. 8: Calculated radial profiles of 2^3S profile at the discharge current of 20, 40, and 60 A.

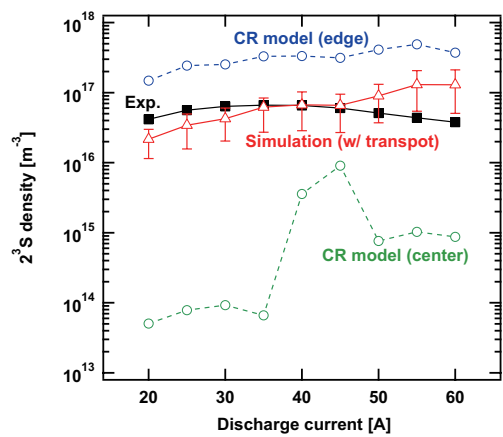


FIG. 9: Comparisons of experimentally obtained and calculated 2^3S densities as a function of the discharge current.